Strain regulation for Phase-Pure and Stable Wide-Bandgap $FAPbBr_3$ Perovskites Solar Cells

Materials & Methods

Materials

The experiments used all the reagents without any treatment. Glass substrates with indium tin oxide (ITO) were bought at Systec Technology. Lead bromide ($PbBr_2$, 99.99%) was purchased from TCI, followed by formamidinium bromide (FABr, 99.99%) from Greatcell Solar Materials. [6,6]-Phenyl-C_{61}-butyric acid methyl ester (PCBM, 99.0%) and nickel oxide (NiO_x) nanoparticles were purchased from Advanced Election Technology Co., Ltd. 2-(3,6-diiodo-9H-carbazol-9-yl)ethyl phosphonic acid (I-2PACz) was purchased from Ningbo Borun New Materials Technology Co., Ltd. Dimethyl sulfoxide (DMSO, anhydrous, 99.9%), N,N-dimethylformamide (DMF, anhydrous, 99.8%), benzene ether (anisole, anhydrous, 99.7%), and chlorobenzene (CB, anhydrous, 99.8%) were purchased from Sigma-Aldrich. Phenethylammonium bromide (PEABr, %), ethylenediammonium dibromide ($EDABr_2$, %), and 4-chlorobenzenesulfonate (4Cl-BZS) were purchased from Sigma.

Solution Preparation

NiO_x solution was made by dispersing the NiO_x nanoparticles in deionized water at a concentration of 20 mg mL^{-1} and filtered using a 0.22 μm syringe filter. I-2PACz solution was prepared by dissolution of I-2PACz in anhydrous methanol at concentration of 0.5 mg mL^{-1} and then filtered through 0.22 μm PTFE syringe filter.

The stoichiometric ratio of formamidinium bromide (FABr) and lead bromide ($PbBr_2$) was dissolved in a mixed solvent of DMF and DMSO (4:1, v/v) to obtain the $FAPbBr_3$ perovskite precursor solution (1.0 M). In order to determine the impact of additive concentration, 4-chlorobenzenesulfonate (4Cl-BZS) was added to the precursor solution in various concentrations (0.5, 1.0, 1.5, and 2.0 mg). A 0.22 μm PTFE syringe filter was used to filter all perovskite precursor solutions before deposition.

To prepare the PEABr-$EDABr_2$ solution to use in post treatment, 1 mg of PEABr and 0.5 mg of EDABr2 were dissolved in 1 mL of isopropyl alcohol (IPA) and filtered using a 0.22 μm PTFE syringe filter. PCBM solution was made by dissolving 20 mg PCBM in 1 mL of chlorobenzene (CB) and filtered using 0.22 μm PTFE syringe filter.

Device fabrication

The devices were made in an inverted p-i-n structure with the structure of ITO/NiOx/I-2PACZ/Perovskite/PEABr:$EDABr_2$/PCBM/PEIE/SnO_x/Ag. Indium tin oxide (ITO) coated glasses were used as substrates. The ITO glass substrates were ultrasonically cleaned in detergent, deionized water, acetone and isopropanol for 20 min. Prior to deposition of the layers, the substrates were subjected to 25 min of exposure to ultraviolet ozone to make the surfaces clean.

The NiO_x layer was spin coated on the ITO substrates using a 20 mg mL^{-1} NiO_x solution at 3000 rpm over a period of 25 s and annealed at 120 °C in air. The substrates were transferred into a nitrogen filled glovebox after annealing. I-2PACz layer was spin-coated on NiO_x film at 3000 rpm and 30 s and annealed at 100 ˚C for 10 min. The $FAPbBr_3$ perovskite films with and without 4Cl-BZS were prepared by spin coating the precursor solution at 500 rpm for 10 s, followed by 4000 rpm for 30 s, Anisole as an antisolvent was dropped on the substrate at 7 s prior to the completion

of the spinning process. The films were then annealed at 100 ˚C 15 min. To modify the surface, the filtered PEABr $EDABr_2$ mixed solution was spin-coated on the perovskite films at 3000 rpm within 30 s after which the samples were annealed at 100 ˚C in 5 min. PCBM layer was then subsequently spin-coated at 1000 rpm over 40 s. Next, a 20 nm SnO_x layer was deposited by atomic layer deposition (ALD) at 100 ˚C using tetrakis(dimethylamino)tin (IV) (99.9999%) as the precursor. Lastly, a 100 nm Ag electrode was deposited by thermal evaporation under a vacuum of 5×10^{-4} Pa.

Characterizations

A EVASTAR E3 X-ray diffractometer was used to collect XRD patterns. The grazing incidence X-ray diffraction (GIXRD, Rigaku SmartLab) was utilized to characterize the residual tensile thermal stress of perovskite films. X-ray photoelectron spectroscopy (XPS) was performed by Thermo K-Alpha+. Fourier-transform infrared (FTIR) spectra were measured with a Shimadzu IR Affinity-1 spectrometer. A Shimadzu UV-2900i spectrophotometer was used to measure the UV-Vis absorption spectra. Scanning Electron Microscopy (SEM) was performed using a Zeiss Gemini-360 ultra-high-resolution field-emission SEM To assess film morphology. A Horiba LabRAM HR Evolution spectrometer with a 325 nm excitation laser was used to record steady-state PL spectra. TRPL was measured at the same wavelength of excitation. Photovoltaic performance of the devices was analyzed using a Keysight 2901BL source meter at AM 1.5G (100 mW cm^{-1}). A solar simulator (SS-X50, Enli Tech) was used for the measurements, and the light intensity was calibrated with a KG1 reference cell prior to each test. *J-V* characteristics, stabilized power output (SPO), and light-intensity-dependent V_{oc} measurements were performed with a shadow mask whose active area was 0.049 cm^2 in direct contact with the glass side of the devices. The measurements of the external quantum efficiency (EQE) were carried out with the QE-R

system of Enli Technology. Measures of EIS and Mott Schottky were conducted on a CHI 660E electrochemical workstation. EIS measurements were done in the dark with a bias of 1 V and Mott-Schottky plots were taken at a frequency of 10 kHz.

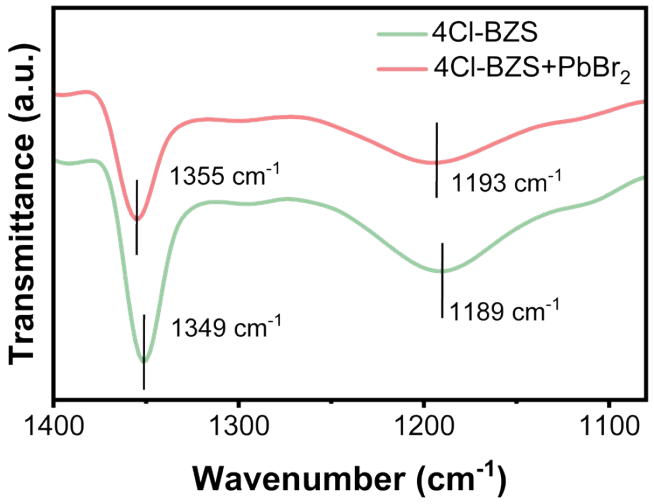

Figure S1. FTIR spectra for 4Cl-BZS additives with and without $PbBr_2$.

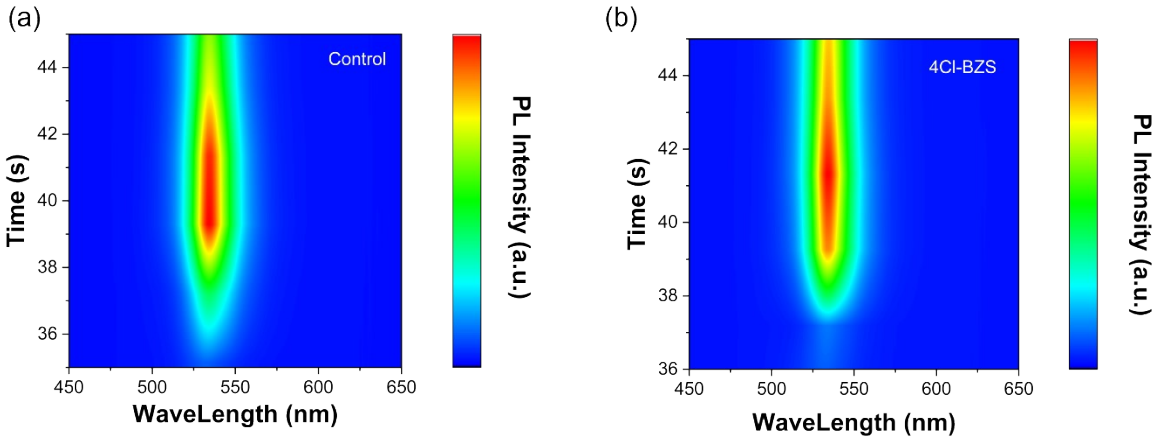

Figure S2. In suit PL spectra during spin coating of the control and 4Cl-BZS films.

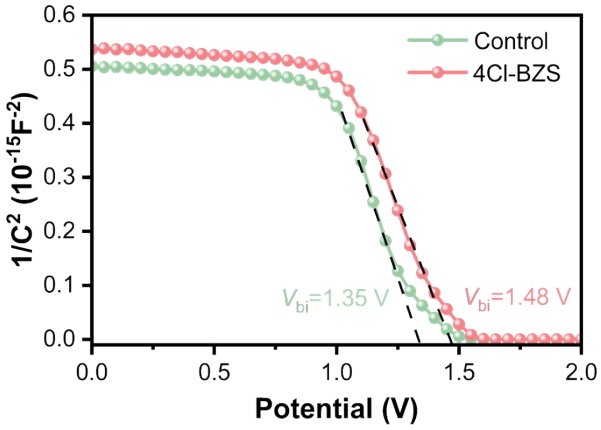

Figure S4. Mott-Schottky curves of the control and 4Cl-BZS devices.

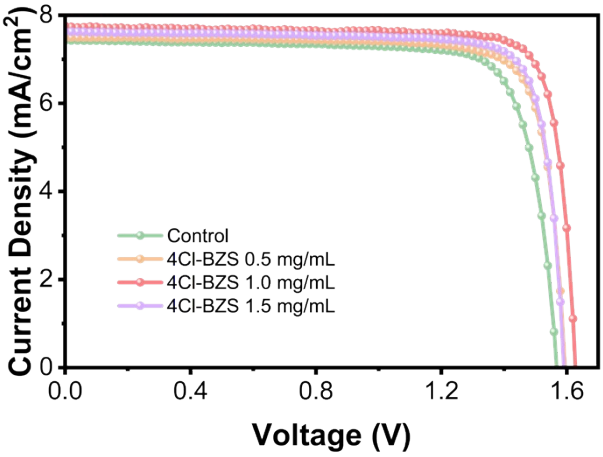

Figure S5. *J-V* curves of different concentrations of 4Cl-BZS devices

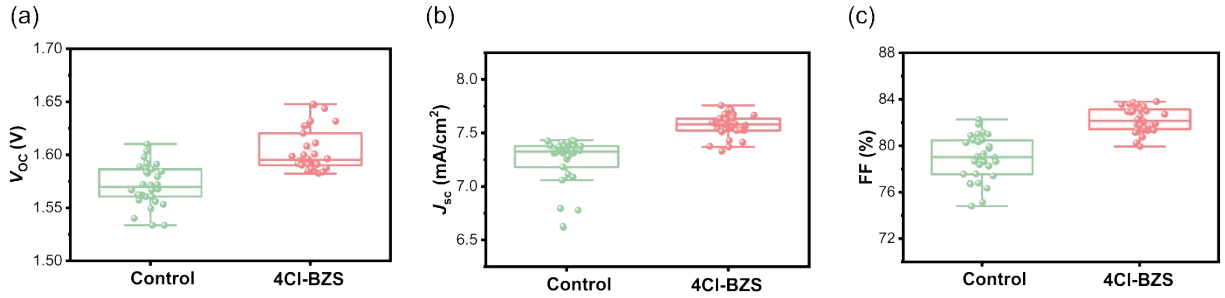

Fig. S6. (a) Open circuit voltage (V_{OC}), (b) Short circuit current density (J_{sc}), (c) Fill Factor (FF) parameters of control and 4Cl-BZS modified devices.

Table S1. The TRPL decay profiles curves fitting by bi-exponential decay function.

Sample	τ_1 (ns)	A_1	τ_2 (ns)	A_2	τ_{avg} (ns)
control	82.11	91814.25	503.00	645.15	99.49
4Cl-BZS	190.32	3952.85	725.16	667.87	399.79

Table S2. V_{TFL} and N_t from the space charge limited current measurements of the electron-only devices.

Devices	ε_0 ($\times 10^{-12}$ F m^{-1})	ε	V_{TFL} (V)	e ($\times 10^{-19}$ C)	L (nm)	N_t ($\times 10^{16}$ cm^{-3})
Control	8.85	43.6	0.56	1.6	380	1.87
4Cl-BZS	8.85	43.6	0.43	1.6	380	1.43

Table S3. The summary of the representative perovskite photovoltaics of p-i-n $FAPbBr_3$

Structure	V_{OC}, V	J_{SC}, mA/cm^2	FF, %	PCE, %	Method	Ref
FTO/NiO/$FAPbBr_3$/ZnO/Ag	1.23	9.90	55.0	6.73	One-step	1
FTO/PEDOT:PSS/$FAPbBr_3$/PCBM/ZnO/Ag	1.35	10.30	59.7	8.30	One-step	2
ITO/NiO_x/$FAPbBr_3$/PCBM/ZnO/BCP/Ag	1.38	8.80	74.0	8.98	One-step	3
ITO/P3CT/$FAPbBr_3$/PCBM/C_{60}/BCP/Cu (TET)	1.48	8.50	66.5	8.33	Two-step	4
ITO/NiO_x/2PACz/$FAPbBr_3$/C_{60}/BCP/Ag	1.45	8.62	69.7	8.71	One-step	5
ITO/PTAA/$FAPbBr_3$/OTS/C_{60}/BCP/Cu	1.48	7.31	68.6	7.49	One-step	6
FTO/NiO_x/I-2PACz/$FAPbBr_3$/C_{60}/BCP/Ag	1.51	9.16	80.6	11.14	One-step	7
FTO/NiO_x/3,7-POPA/$FAPbBr_3$/C_{60}/BCP/Ag	1.51	9.15	77.8	10.79	One-step	8
FTO/NiO_x/ I-2PACz/$FAPbBr_3$/PCBM/SnO_x/Ag	1.63	7.76	83.7	10.56	One-step	In this work

Reference

1. A. S. Subbiah, N. Mahuli, S. Agarwal, M. F. A. M. van Hest and S. K. Sarkar, Towards All-Inorganic Transport Layers for Wide-Band-Gap Formamidinium Lead Bromide-Based Planar Photovoltaics, *Energy Tech*, 2017, **5**, 1800–1806.
2. A. S. Subbiah, S. Agarwal, N. Mahuli, P. Nair, M. Van Hest and S. K. Sarkar, Stable p–i–n $FAPbBr_3$ Devices with Improved Efficiency Using Sputtered ZnO as Electron Transport Layer, *Adv Materials Inter*, 2017, **4**, 1601143.
3. S. B. Shivarudraiah, N. Tewari, M. Ng, C.-H. A. Li, D. Chen and J. E. Halpert, Optically Clear Films of Formamidinium Lead Bromide Perovskite for Wide-Band-Gap, Solution-Processed, Semitransparent Solar Cells, *ACS Appl. Mater. Interfaces*, 2021, **13**, 37223–37230.
4. S. Li, C. Deng, L. Tao, Z. Lu, W. Zhang and W. Song, Crystallization Control and Defect Passivation via a Cross-Linking Additive for High-Performance $FAPbBr_3$ Perovskite Solar Cells, *J. Phys. Chem. C*, 2021, **125**, 12551–12559.
5. H. Zhu, W. Wu, Y. Wu, D. Zhang, H. Zhan, Y. Cheng, L. Wang and C. Qin, δ-Phase Management of FAPbBr3 for Semitransparent Solar Cells, *Advanced Optical Materials*, 2023, **11**, 2202827.
6. Q. Li, Y. Zheng, X. Guo, G. Zhang, G. Ding, Y. Shi, F. Li, M. Sun and Y. Shao, Interface Engineering Enhances the Photovoltaic Performance of Wide Bandgap $FAPbBr_3$ Perovskite for Application in Low-Light Environments, *Adv Funct Materials*, 2023, **33**, 2303729.
7. H. Zhu, Z. Xu, Z. Zhang, S. Lian, Y. Wu, D. Zhang, H. Zhan, L. Wang, L. Han and C. Qin, Improved Hole-Selective Contact Enables Highly Efficient and Stable $FAPbBr_3$ Perovskite Solar Cells and Semitransparent Modules, *Advanced Materials*, 2024, **36**, 2406872.
8. A. Dolgormaa, Y. Wu, Z. Xu, H. Zhu, Y. Zhang, S. Lian, W. Wu, B. Li, H. Zhan, L. Wang and C. Qin, High-Efficiency and Stable $FAPbBr_3$ Perovskite Solar Cells Enabled by 3,7-POPA: A Multifunctional Phenoxazine-Based Self-Assembled Monolayers, *Adv Funct Materials*, 2026, **36**, e16065.